Spectroscopic and Excited-State Properties of Tri-9-anthrylborane II: Electroabsorption and Electrofluorescence Spectra

Noboru Kitamura,*,† Eri Sakuda,† Tomokazu Yoshizawa,‡ Toshifumi Iimori,‡ and Nobuhiro Ohta*,‡

Division of Chemistry, Graduate School of Science, Hokkaido University, 060−0810 Sapporo, Japan, and Research Institute for Electronic Science, Hokkaido University, 060−0812 Sapporo, Japan

Received: February 8, 2005; In Final Form: June 22, 2005

Electroabsorption and electrofluorescence spectroscopies were conducted for tri-9-anthrylborane (**TAB**) doped in poly(methyl methacrylate) films (1.0 mol %) to reveal the spectroscopic and excited-state properties of the compound. **TAB** showed three distinct absorption bands: bands I [$(19 - 25) \times 10^3$ cm^{-1}], II [$(25-31) \times 10^3$ cm^{-1}], and III ($>31 \times 10^3$ cm^{-1}). The electroabsorption spectrum demonstrated that the electronic transitions in bands I and III accompanied electric dipole moment changes ($\Delta\mu$), while the change in the molecular polarizability contributed mainly to electroabsorption band II. Because of the similarities of the electroabsorption spectrum of band II with that of anthracene itself, band II was assigned to the electronic transition to the locally excited (LE) state of the anthryl group. On the other hand, bands I and III were best described by the electronic transitions to the excited charge-transfer (CT) states. The study demonstrated furthermore that the $\Delta\mu$ value of **TAB** accompanied by the lowest-energy electronic transition was as large as 7.8 D, which agreed very well with that determined by the solvent dependences of the absorption and fluorescence maximum energies of **TAB** (∼8.0 D, ref 1): $\Delta\mu = 7.8-8.0$ D. The results proved explicitly that the excited state of **TAB** was localized primarily on the p orbital of the boron atom. Despite the dipole moment change ($\Delta\mu = 7.8-8.0$ D) for the lowest-energy electronic transition (band I), the electrofluorescence of **TAB** accompanied the change in the molecular polarizability. The spectroscopic and excited-state properties of **TAB** including the curious behavior of the electrofluorescence spectrum as mentioned above were discussed on the basis of theoretical considerations.

Introduction

On the basis of the solvent polarity [$f(X)$] dependences of the spectroscopic and excited-state properties of tri-9-anthrylborane (**TAB**), we concluded that the lowest-energy electronic transition in **TAB** accompanied a large dipole moment change ($\Delta\mu$), and this was attributed to the excited-state electric dipole moment of the molecule (μ_e): $\mu_e \approx \Delta\mu \approx 8.0$ D, as described in detail in the preceding paper in this issue (part I).[1] The μ_e or $\Delta\mu$ value demonstrated, furthermore, that the excited state of **TAB** was localized primarily on the p orbital of the boron atom. Nonetheless, the conclusion, based on the $f(X)$ dependences of the absorption and fluorescence maximum energies of **TAB** alone, might not be warranted because the spectroscopic properties of a molecule are influenced by the various solvent properties in a complicated manner.[2] Furthermore, although we discussed the $f(X)$ dependence of the nonradiative decay rate constant (k_{nr}) of **TAB** on the basis of the energy gap law,[1] the detailed excited-state properties have not yet been revealed. Therefore, more explicit information about the spectroscopic and excited-state properties of **TAB,** other than their solvent effects, is absolutely necessary to understand the characteristics of the molecule. To clarify such issues, we studied the electroabsorption and electrofluorescence spectra of **TAB** in polymer films.

In this paper, we describe the characteristics of the electroabsorption and electrofluorescence spectra of **TAB** doped in poly(methyl methacrylate) films and discuss the origins of the electronic transitions in **TAB**. In practice, we succeeded in analyzing the observed electroabsorption and electrofluorescence spectra of **TAB** and determined the electric dipole moment change upon optical excitation, which was very important to elucidate the nature of the excited state of the compound. Furthermore, we also conducted a theoretical study on the excited states of **TAB**, and these results were compared with experimental observations.

Experimental Section

Principles of Electroabsorption and Electrofluorescence Spectroscopies. Electroabsorption and electrofluorescence spectra (i.e., Stark spectra) provide information about a shift of the molecular level under an external electric field.[3−10] When an electric field with the strength of F is applied to a molecule, each energy level is generally shifted and the magnitude of the shift depends on an electric dipole moment (μ) and a molecular polarizability (α) of the state concerned: the level shift is given by $-\mu F - \alpha F^2/2$. As a result, the transition energy for absorption or fluorescence varies with F. For an isotropic and immobilized sample, an application of F will broaden an isolated transition because of the change in μ following light absorption

* To whom correspondence should be addressed. E-mail: kitamura@sci.hokudai.ac.jp (N.K.); nohta@es.hokudai.ac.jp (N.O.).

† Division of Chemistry, Graduate School of Science, Hokkaido University.

‡ Research Institute for Electronic Science, Hokkaido University.

10.1021/jp050702g CCC: $30.25
Published on Web 07/30/2005

giving rise to a Stark effect line shape, which is approximately the second derivative of the absorption spectrum. If the molecular polarizability varies upon photoexcitation, on the other hand, the Stark effect line shape becomes the first derivative of the absorption spectrum. When the transition moment is affected by F, the Stark effect line shape is the same as the absorption spectrum.

The change in the absorption intensity at wavenumber (ν) in the presence of F, $\Delta A(\nu)$, is given by

$$\Delta A(\nu) = (fF)^2\left[A_x A(\nu) + B_x \nu \frac{\mathrm{d}}{\mathrm{d}\nu}\left(\frac{A(\nu)}{\nu}\right) + C_x \nu \frac{\mathrm{d}^2}{\mathrm{d}\nu^2}\left(\frac{A(\nu)}{\nu}\right)\right] \quad (1)$$

where f is the internal field factor. Coefficient A_x depends on the transition moment polarizability and hyperpolarizability, and B_x and C_x are given as follows

$$B_x = \frac{1}{hc}\left[\frac{\Delta\bar{\alpha}}{2} + \frac{1}{10}(\Delta\alpha_m - \Delta\bar{\alpha})(3\cos^2\chi - 1)\right] \quad (2)$$

$$C_x = \frac{(\Delta\mu)^2}{30h^2c^2}[5 + (3\cos^2\chi - 1)(3\cos^2\xi - 1)] \quad (3)$$

where $\Delta\bar{\alpha} = (1/3)Tr(\Delta\alpha)$ and $\Delta\alpha$ represents the difference in the molecular polarizability between the ground and excited states. $\Delta\alpha_m$ denotes the diagonal component of $\Delta\alpha$ with respect to the direction of the transition moment. χ is the angle between the direction of F and the electric vector of excitation light, and ξ is the angle between the direction of $\Delta\mu$ and the transition dipole moment. On the other hand, the change in the fluorescence intensity under F ($\Delta I_F(\nu)$) is given by replacing $A(\nu)$ and ν in eq 1 by the fluorescence intensity ($I_F(\nu)$) and ν^3, respectively, and the relevant A, B, and C terms are defined similarly to those for absorption measurements.[7] By comparing the electroabsorption and electrofluorescence spectra with the first or second derivative of the relevant absorption and fluorescence spectra, one, therefore, can discuss the μ and α values of a molecule of interest.[3−9]

Experimental Setup. Electroabsorption and electrofluorescence spectroscopies were conducted by using the system and procedures reported previously.[3,4] Briefly, a benzene solution of poly(methyl methacrylate) (PMMA, Aldrich, MW = 1.2×10^5) containing 0.5−1.0 mol % of **TAB** was spin-coated onto the ITO electrode fabricated on a quartz substrate. An aluminum layer was then vacuum deposited onto the **TAB**/PMMA film, and the ITO and Al electrodes were connected with a function generator (SG-4311, Iwatsu) combined with an amplifier (Model 609A, Trek) to apply ac voltage to the electrodes. The electric field-induced change in the absorption or fluorescence intensity was detected with a lock-in-amplifier (SR830, Stanford Research Systems Inc.) at the second harmonic of the modulation frequency. The spectra were obtained under magic angle conditions between the polarization direction of linearly polarized excitation light and that of the applied electric field: $\chi = 54.7°$ in eqs 2 and 3. The experimental setup used in our previous studies was complemented with a Glan−Taylor prism polarizer (CASIX, PGT8210) and a rotatable sample holder for measuring electroabsorption spectra with polarized light.[10] For fluorescence spectroscopy, unpolarized light was used for excitation, and unpolarized fluorescence was detected with a propagation direction perpendicular to that of the excitation light. The **TAB** used in this study was the essentially the same with that reported in the previous paper.[1]

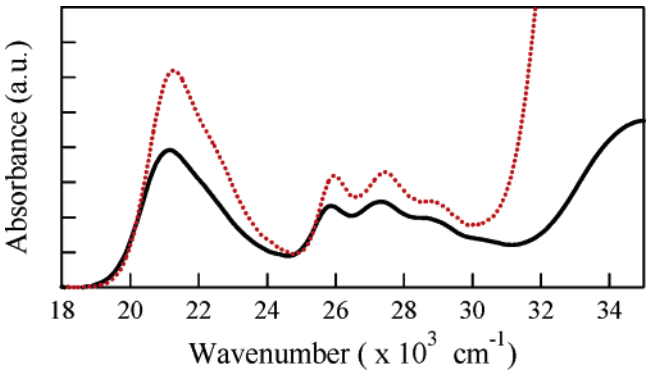

Figure 1. Absorption spectra of **TAB** in a PMMA film (1.0 mol %, shown in black) and THF (5.8×10^{-6} M, shown in red).

Results and Discussion

Absorption and Fluorescence Spectra of TAB in PMMA Films. Figure 1 shows the absorption spectrum of **TAB** (1.0 mol %) in a PMMA film (shown in black) together with that in THF (5.8×10^{-6} M, shown in red). In the wavenumber region studied [$\nu = (17-36) \times 10^3$ cm^{-1}], **TAB** showed three main absorption bands: a broad low-energy band peaking at $\nu_a = 21.2 \times 10^3$ cm^{-1} [band I, $(19-25) \times 10^3$ cm^{-1}], a relatively structured anthracene-like band [band II, $(25-31) \times 10^3$ cm^{-1}], and a broad high-energy band peaking at $\nu_a = 35.0 \times 10^3$ cm^{-1} (band III, $>31 \times 10^3$ cm^{-1}). The spectral band shapes and the ν_a values of the three absorption bands of **TAB** in the PMMA film were very similar to those observed in THF or other aprotic solvents.[1] The absorption characteristics of **TAB** are thus concluded to be insensitive to the solvent or microenvironment. On the other hand, as can be seen from the data shown later, the **TAB** in the PMMA film showed a fluorescence maximum at $\nu_f = 19.0 \times 10^3$ cm^{-1}. Although the fluorescence maximum energy of **TAB** was shown to be very sensitive to solvent polarity,[1] both the spectral band shape and the ν_f value in the PMMA film were almost the same as those observed in ethyl acetate ($\nu_f = 19.0 \times 10^3$ cm^{-1}),[1] reflecting the microenvironmental polarity around **TAB** in the film. These results indicate that no specific interaction between **TAB** and PMMA takes place even in the solid state and that **TAB** is dispersed homogeneously in the film. Therefore, we can discuss the spectroscopic and excited-state properties of **TAB** on the basis of the electroabsorption and electrofluorescence spectra measured in PMMA films.

Electroabsorption and Electrofluorescence Spectra of TAB in PMMA Films. The electroabsorption and electrofluorescence spectra of **TAB** doped in PMMA films (1.0 mol %, $F = 1.0$ MV/cm) are shown in Figures 2 and 3, respectively. For the absorption and electroabsorption spectra, those of bands I [$(17-25) \times 10^3$ cm^{-1}], II [$(24-30) \times 10^3$ cm^{-1}], and III [$(29-36) \times 10^3$ cm^{-1}] are also shown separately in Figure 2b, c, and d, respectively, for clarity. The top and bottom panels in each figure represent the absorption and electroabsorption spectra, respectively (shown in black), and the middle panel shows the first (shown in red) and second derivatives (shown in blue) of the absorption spectrum. The red curve shown in each bottom panel represents the best fit of the electroabsorption spectrum by simulations. In Figure 3, similarly, the fluorescence and electrofluorescence spectra of **TAB** are shown in the top and bottom panels (shown in black), respectively, while the first (shown in red) and second derivatives (shown in blue) of the fluorescence spectrum are shown in the middle panel. In the bottom panel, the simulated electrofluorescence spectrum is also shown in red.

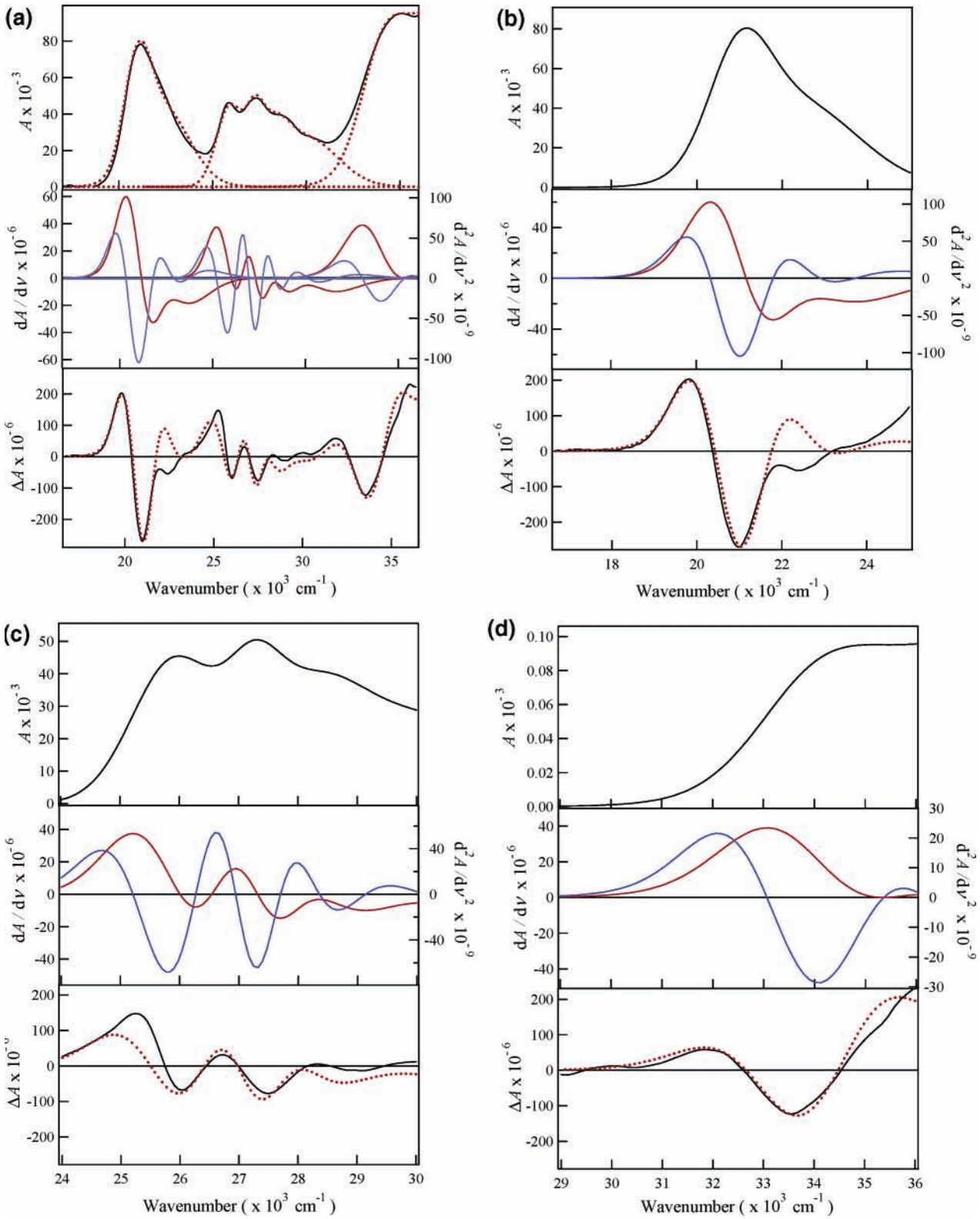

Figure 2. Absorption (top panel) and electroabsorption spectra (bottom panel, shown in black) of **TAB** doped in PMMA films (1.0 mol %, F = 1.0 MV) in the ν range of (18−36) × 10^3 cm^{-1} (a). The middle panel shows the first (red) and second derivatives (blue) of the absorption spectrum; the first and second derivatives of each band (bands I, II, and III) are superimposed. The red spectrum in the bottom panel represents the simulated one. Panels b, c, and d show separately the spectra of bands I, II, and III, respectively, for clarity.

In the spectral region of band I (Figure 2b), the electroabsorption spectrum was best simulated using the dominant contribution of the second derivative of the absorption spectrum, while the first derivative of the absorption spectrum contributed mainly to electroabsorption band II (Figure 2c). On the other hand, the electroabsorption spectrum of band III was reproduced well by the second derivative of the relevant absorption spectrum (Figure 2d), similar to band I. It is worth noting that the first and second derivatives result from the changes in an electric dipole moment ($\Delta\mu$) and a molecular polarizability (α),

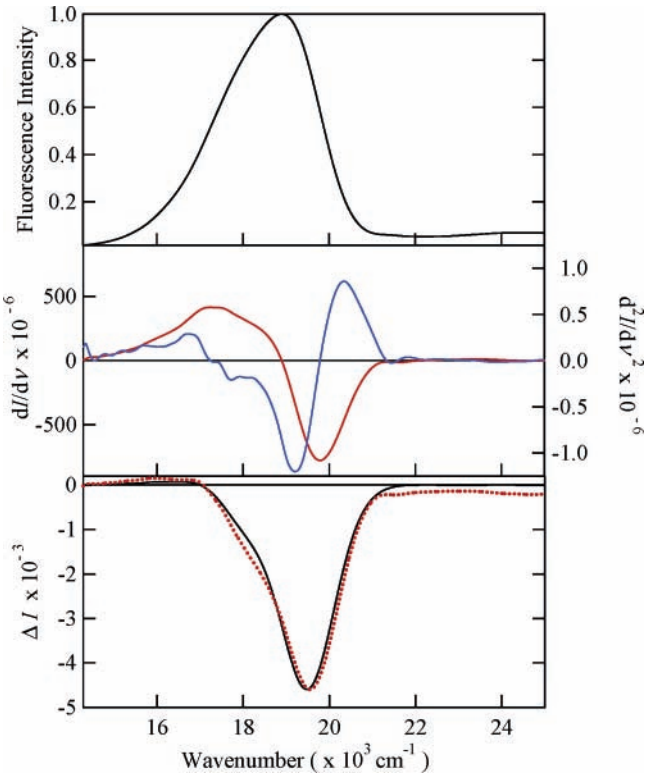

Figure 3. Fluorescence (top panel) and electrofluorescence spectra (bottom panel, shown in black) of **TAB** doped in PMMA films (1.0 mol %, $F = 1.0$ MV). The middle panel shows the first (red) and second derivatives (blue) of the fluorescence spectrum. The red spectrum in the bottom panel represents the simulated one.

respectively (eq 1). The total electroabsorption spectrum of **TAB** in the ν range of $(18-36) \times 10^3$ cm^{-1} was then reasonably simulated by the superposition of bands I ($\Delta\mu$), II (α), and III ($\Delta\mu$), as shown in the bottom panel in Figure 2a (shown in red), though the agreements between the observed and simulated spectra in the ν regions overlapping the two transitions (i.e., band I−II and band II−III) were not necessarily good enough. Nonetheless, the present results showed clearly that the two absorption bands (I and II) were essentially different transitions. Because the absorption spectrum of band II was very similar to that of anthracene itself,[11] band II could be assigned to the transition to the locally excited state (LE) of the anthryl group in **TAB** as discussed in the following section.

On the other hand, Figure 3 reveals that the first derivative of the fluorescence spectrum accounts for the observed electrofluorescence spectrum (change in α). It is worth noting, furthermore, that the fluorescence of **TAB** is quenched by the external electric field: the fluorescence intensity change in the minus sign in the bottom panel of Figure 3. This indicates that the radiative rate constant of **TAB** at the emitting state becomes smaller, the nonradiative rate constant becomes larger, or both in the presence of an electric field.

On the basis of the analysis of the present experimental observations by eq 1, we determined the value of $\Delta\mu$ for the lowest-energy electronic transition (band I) to be 7.8 D, which agreed quite well with that determined by the $f(X)$ dependence of the $\nu_a - \nu_f$ value (~8.0 D).[1] Because the electric dipole moment in the ground-state of **TAB** (μ_g) has been shown to be almost zero, the large $\Delta\mu$ value accompanied by the electronic transition is responsible for the excited-state dipole moment (μ_e) of **TAB**: $\Delta\mu \approx \mu_e = 7.8-8.0$ D. The results support our conclusion that the excited state of **TAB** is localized primarily on the vacant p orbital of the boron atom. Thus, the lowest-

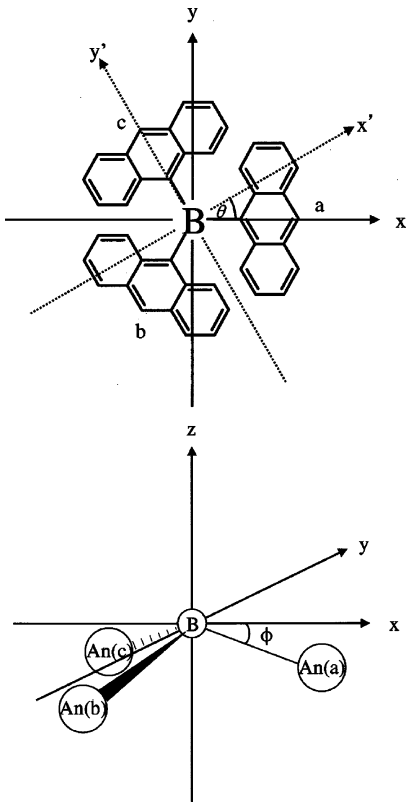

Figure 4. Schematic representations of the geometrical structures of **TAB**.

excited state of **TAB** is best characterized by a charge-transfer (CT) state.

Theoretical Considerations and Their Implications to the Spectroscopic and Excited-State Properties of TAB. Our experiments demonstrated that band I could be assigned to a CT transition. It is worth noting that such a conclusion does not contradict the results obtained via spectroscopic and theoretical work on several triarylboranes; the derivative shows an intramolecular CT transition from the HOMO of the aryl group to the vacant p orbital of the boron atom.[12−15] For example, the absorption spectrum of triphenylborane exhibits a CT band at 34.8×10^3 cm^{-1} (287 nm), and the band observed at 42.0×10^3 cm^{-1} (238 nm) has been assigned to the transition to the locally excited (LE) state of the phenyl group.[12] Analogous CT and LE bands also appear in the spectrum of tri(1-naphthyl)borane.[13] Similarly, in the case of **TAB**, band II can be assigned to the LE transition in the anthryl group as described above. Therefore, **TAB** also exhibits both CT and LE bands analogous to other triarylborane derivatives. Our assignments of the electronic transitions in Figure 2 are thus very reasonable. However, more explicit descriptions of the excited state of **TAB** are certainly necessary to discuss the spectroscopic characteristics of the compound. Therefore, in the following, we briefly describe the theoretical considerations of the excited CT state of **TAB**.

The stationary states for the CT transition in **TAB** at the first order can be derived from mixing of the zero-order states, originated from the charge transfer between each anthryl group and the boron atom. We distinguish the three anthryl groups in **TAB** by labeling them a, b, and c, as shown in Figure 4a. The zero-order basis set for the CT state can be then expressed by eq 4

$$|l,m,n\rangle = |(C_{14}H_9)_a^{\,l}\rangle|(C_{14}H_9)_b^{\,m}\rangle|(C_{14}H_9)_c^{\,n}\rangle|B^-\rangle \qquad (4)$$

where $|B^-\rangle$ is the electronic state of the boron atom whose π-type p orbital is occupied by one electron and *l*, *m*, and *n* indicate the localized electronic states of the anthryl groups at a, b, and c, respectively. Denoting the neutral and ionized states of the anthryl group in **TAB** by 0 and +, respectively, we obtain three basis functions: $|+, 0, 0\rangle$; $|0, +, 0\rangle$; and $|0, 0, +\rangle$. By taking a linear combination of these three basis functions, we can construct the first-order stationary states.

The x-ray crystal structure analysis of **TAB** reported by Yamaguchi et al. has shown that the three carbon−boron bonds are in a planar configuration,[16] and therefore, **TAB** belongs to the D_3 point group in the ground state. The electronic ground state of **TAB** is expressed as in eq 5

$$|\psi_G\rangle = |(C_{14}H_9)_a^{\ 0}\rangle|(C_{14}H_9)_b^{\ 0}\rangle|(C_{14}H_9)_c^{\ 0}\rangle|B\rangle \tag{5}$$

where $|B\rangle$ is the electronic state of the boron atom with an unfilled π-type p orbital, whose state has *A* symmetry. On the other hand, one can assume that the three carbon−boron bonds in the excited CT state are nonplanar because of an sp^3-type configuration of the boron atom when the vacant p orbital is filled by one electron.[17] Therefore, **TAB** in the excited CT state belongs to a C_3 point group, and we can apply the C_3 selection rules for photoexcitation to the CT state. In this case, we may write the symmetry-adapted CT states as

$$|\psi_A\rangle = \frac{1}{\sqrt{3}}\{|+, 0, 0\rangle + |0, +, 0\rangle + |0, 0, +\rangle\} \tag{6a}$$

$$|\psi_{E(1)}\rangle = \frac{1}{\sqrt{6}}\{2|+, 0, 0\rangle - |0, +, 0\rangle - |0, 0, +\rangle\} \tag{6b}$$

$$|\psi_{E(2)}\rangle = \frac{1}{\sqrt{2}}\{|0, +, 0\rangle - |0, 0, +\rangle\} \tag{6c}$$

where we label these functions according to the symmetry species of the C_3 point group.

In the first-order approximation, we can calculate the dipole moments of the three CT states (eq 6) by taking a vectorial sum of the dipole moments of the basis functions. The dipole moment operator for the basis functions is taken as

$$\vec{\mu}_{lmn} = -q_{lmn}e\vec{r}_{lmn} \tag{7}$$

where *e* is an elementary electric charge. q_{lmn} represents the amount of a charge transferred from the anthryl group to the boron atom, and $\vec{r}_{lmn} = (x, y, z)$ is the positional vector from the center of the anthryl cation to the boron atom. Using $q_{+00} = q_{0+0} = q_{00+} \equiv q$ and $|\vec{r}_{+00}| = |\vec{r}_{0+0}| = |\vec{r}_{00+}| \equiv R$, we may calculate the dipole moments of three zero-order states as in eqs 8−10

$$\left.\begin{aligned} qe\langle + 00|\hat{x}| + 00\rangle &= qeR\cos\phi \\ qe\langle + 00|\hat{y}| + 00\rangle &= 0 \\ qe\langle + 00|\hat{z}| + 00\rangle &= -qeR\sin\phi \end{aligned}\right\} \begin{matrix} (8a)\\ (8b)\\ (8c)\end{matrix}$$

$$\left.\begin{aligned} qe\langle 0 + 0|\hat{x}|0 + 0\rangle &= -\frac{1}{2}qeR\cos\phi \\ qe\langle 0 + 0|\hat{y}|0 + 0\rangle &= -\frac{\sqrt{3}}{2}qeR\cos\phi \\ qe\langle 0 + 0|\hat{z}|0 + 0\rangle &= -qeR\sin\phi \end{aligned}\right\} \begin{matrix} (9a)\\ (9b)\\ (9c)\end{matrix}$$

$$\left.\begin{aligned} qe\langle 00 + |\hat{x}|00 + \rangle &= -\frac{1}{2}qeR\cos\phi \\ qe\langle 00 + |\hat{y}|00 + \rangle &= \frac{\sqrt{3}}{2}qeR\cos\phi \\ qe\langle 00 + |\hat{z}|00 + \rangle &= -qeR\sin\phi \end{aligned}\right\} \begin{matrix} (10a)\\ (10b)\\ (10c)\end{matrix}$$

In eqs 8−10, ϕ is the pyramidal angle of the carbon−boron bonds defined as in Figure 4b. The dipole moment of the *A* symmetry state can be calculated as

$$qe\langle\psi_A|\vec{r}|\psi_A\rangle = \begin{pmatrix} 0 \\ 0 \\ -qeR\sin\phi \end{pmatrix} \tag{11}$$

To calculate the dipole moments of the *E* symmetry states, we take a linear combination of the two degenerated states

$$|\Psi\rangle = c_1|\psi_{E(1)}\rangle + c_2|\psi_{E(2)}\rangle \tag{12}$$

where c_1 and c_2 are the coefficients. We now consider another Cartesian coordinate system, which rotates around the *z* axis by θ in the counterclockwise direction

$$\begin{pmatrix} x' \\ y' \\ z' \end{pmatrix} = \begin{pmatrix} \cos\theta & \sin\theta & 0 \\ -\sin\theta & \cos\theta & 0 \\ 0 & 0 & 1 \end{pmatrix}\begin{pmatrix} x \\ y \\ z \end{pmatrix} \tag{13}$$

The x' and y' components of the dipole moment in this rotated axis system can be calculated as in eqs 14 and 15

$$qe\langle\Psi|\hat{x}'|\Psi\rangle = qe\frac{R}{2}\cos\phi\{(c_1^{\ 2} - c_2^{\ 2})\cos\theta + 2c_1c_2\sin\theta\} \tag{14}$$

$$qe\langle\Psi|\hat{y}'|\Psi\rangle = qe\frac{R}{2}\cos\phi\{(-c_1^{\ 2} + c_2^{\ 2})\sin\theta + 2c_1c_2\cos\theta\} \tag{15}$$

We now take the coefficients in the form

$$c_1 = \cos\alpha \tag{16}$$

$$c_2 = \sin\alpha \tag{17}$$

where α is a parameter. One can show that the y' component becomes zero at $\alpha = \theta/2$

$$\langle\Psi_1|\hat{y}'|\Psi_1\rangle = 0 \tag{18}$$

where

$$|\Psi_1\rangle = \cos\frac{\theta}{2}|\psi_{E(1)}\rangle + \sin\frac{\theta}{2}|\psi_{E(2)}\rangle \tag{19}$$

The x' component of the dipole moment is then given by

$$qe\langle\Psi_1|\hat{x}'|\Psi_1\rangle = qe\frac{R}{2}\cos\phi \tag{20}$$

We consider another set of the coefficients which is orthogonal to the set in eqs 16 and 17

$$|\Psi_2\rangle = -\sin\frac{\theta}{2}|\psi_{E(1)}\rangle + \cos\frac{\theta}{2}|\psi_{E(2)}\rangle \tag{21}$$

This state yields eqs 22 and 23

$$qe\langle\Psi_2|\hat{x}'|\Psi_2\rangle = -qe\frac{R}{2}\cos\phi \tag{22}$$

$$qe\langle\Psi_2|\hat{y}'|\Psi_2\rangle = 0 \tag{23}$$

The z' component of the dipole moment is given in eq 24

$$qe\langle\Psi_1|\hat{z}'|\Psi_1\rangle = qe\langle\Psi_2|\hat{z}'|\Psi_2\rangle = -qeR\sin\phi \tag{24}$$

Thus, we can calculate the dipole moment of the *E* symmetry states as

$$|\vec{\mu}_E| = qeR\left(1 - \frac{3}{4}\cos^2\phi\right)^{1/2} \tag{25}$$

It should be noted that an external electric field can lift the degeneracy of the *E* symmetry states, and the dipole moment of each state is given by $\pm|\vec{\mu}_E|$ for any direction of the external field. If we assume that the deviation of the structure of **TAB** from the planar configuration at the boron atom is small (i.e., $\phi \approx 0°$), the dipole moments of the degenerated CT states with *E* symmetry are given by the following equation

$$|\vec{\mu}_E| = \frac{qeR}{2} \tag{26}$$

and the excited *A* state, $|\psi_A\rangle$, and the ground state, $|\psi_G\rangle$, yield zero dipole moment.

The polarizability of the CT states can be also calculated as the expectation value of the polarizability operator, $\hat{\alpha}$. For the $|\psi_A\rangle$ state, we can calculate the polarizability as in eq 27

$$\langle\psi_A|\hat{\alpha}|\psi_A\rangle = \frac{1}{3}(\langle + 00|\hat{\alpha}| + 00\rangle + \langle 0 + 0|\hat{\alpha}|0 + 0\rangle + \langle 00 + |\hat{\alpha}|00 + \rangle) \tag{27}$$

where we have omitted the cross terms of the matrix elements. If we make a crude approximation that the isotropic component of the polarizability tensor is dominant over any other anisotropic one, all three terms in the right hand side of eq 27 can be regarded as scalars. Consequently, the *A* state possesses the nonzero polarizability as given in eq 28

$$\alpha_0 \equiv \langle + 00|\hat{\alpha}| + 00\rangle = \langle 0 + 0|\hat{\alpha}|0 + 0\rangle = \langle 00 + |\hat{\alpha}|00 + \rangle \tag{28}$$

One can show that the other two degenerated states also have the same polarizability value, α_0.

On the basis of the present model for the electronic structures of **TAB**, the electroabsorption (Figure 2) and electrofluorescence spectra (Figure 3) can be discussed as follows. The electroabsorption spectrum of band II (Figure 2c) showed a molecular polarizability change. The results are very similar to the electroabsorption spectrum of anthracene,[11] indicating that band II is assigned to the transition to the LE state of the anthryl group in **TAB** as described before. On the other hand, the electronic transition in band I (Figure 2b) accompanied a dipole moment change and the relevant $\Delta\mu$ value was estimated to be 7.8−8.0 D. Therefore, we conclude that band I is assigned to the transition to the degenerated CT states, whose characters are described above. From the x-ray crystal structure analysis of **TAB**, we obtained $R = 3.03$ Å as the distance between the boron atom and the center of the anthryl group.[16] By approximating the planar geometry of the three bonds on the boron atom (i.e., $\phi = 0°$) and by putting the value $|\Delta\vec{\mu}| \approx |\vec{\mu}_E| = 7.8$ D into eq 26, we can estimate the amount of charge transferred from the anthryl group to the boron atom to be $q = \sim 1.0$. It is worth noting that, if we take the sp^3 hybrid structure of the boron atom, the ϕ value is 19.5° and eq 25 yields $q = 0.89$ for the CT state of *E* symmetry. These considerations indicate that nearly one electron is transferred from the anthryl group to the boron atom in the excited CT state of **TAB** with *E* symmetry. It is pertinent to note, furthermore, that band III, observed at $\nu_a = 35.0 \times 10^3$ cm^{-1} (Figure 2d), shows similar Stark effects to band I. Therefore, the results strongly indicate that band III should be responsible for a certain CT state possessing a dipole moment.

On the other hand, the electrofluorescence spectrum of **TAB** showed a large change in the molecular polarizability following the fluorescence process, in contrast to the Stark effects on absorption band I. The results can be explained by the assumption that the lowest-excited singlet state (i.e., the emitting state of fluorescence) is the $|\psi_A\rangle$ state but not the degenerate $|\psi_E\rangle$ states. In such a case, the excited state produced by optical excitation of band I is considered to relax to the lowest $|\psi_A\rangle$ state via internal conversion. Note that the fluorescence generally emits from the lowest-excited singlet state. Therefore, since both the excited $|\psi_A\rangle$ state and the ground state of **TAB** have no dipole moment, the only factor governing the electrofluorescence of the compound is the change in the molecular polarizability, as observed in the present experiments.

The transition dipole moment from the ground state to the excited $|\psi_A\rangle$ state orients parallel to the *z* axis, while those to the degenerated excited $|\Psi_1\rangle$ and $|\Psi_2\rangle$ states (i.e., $|\psi_E\rangle$ states) lie in the $x-y$ plane (Figure 4). It has been reported that the CT absorption bands of other triarylborane derivatives are responsible for the transitions to the degenerated *E* symmetry excited states, while the transition strength from the ground state to the *A* symmetry excited state is very small.[12−15] Therefore, **TAB** will show a similar optical transition; the transition from the ground state to the $|\psi_E\rangle$ states is strongly allowed, while the transition to the $|\psi_A\rangle$ state is nearly forbidden. The present conclusion of the nearly-zero absorption intensity to the $|\psi_A\rangle$ state does not contradict the prediction of the planar excited-state geometry of **TAB** with D_3 point group.

The forbidden character of the fluorescent transition from the excited $|\psi_A\rangle$ state to the ground state can be checked by comparing the observed radiative rate constant (k_f) of **TAB** with the value calculated from the absorption spectrum of band I. One can calculate the radiative rate constant, $k_f{}^0$, on the basis of eq 29[18]

$$k_f{}^0 = 3.0 \times 10^{-9}\nu_a{}^2\int\epsilon d\nu \tag{29}$$

In THF, for example, the $k_f{}^0$ value calculated from the absorption spectrum of band I ($\epsilon = 2.14 \times 10^4$ M^{-1} cm^{-1} at $\nu_a = 21.2 \times 10^3$ cm^{-1}, see Table 1 and Figure 1 in ref 1) is 1.5×10^8 s^{-1} while the observed k_f value is 1.4×10^7 s^{-1} (see Table 2 in ref 1), demonstrating that the observed k_f value is ∼10 times smaller than $k_f{}^0$. Although both the ϵ and k_f values observed for **TAB** are moderately dependent on the solvent, the k_f value evaluated from the fluorescence quantum yield and lifetime in a given solvent is much smaller than the relevant $k_f{}^0$ value regardless of the solvent. Therefore, the results are very consistent with the assignment that the state emitting the fluorescence is the $|\psi_A\rangle$ state, while absorption band I is assigned to the allowed transition from the ground state to the degenerated $|\psi_E\rangle$ states. Because of the weak transition strength to the $|\psi_A\rangle$ state, the relevant absorption band could be buried in absorption band I and therefore could not be identified with the present experiments.

Conclusions

In this paper, we reported detailed spectroscopic and excited-state properties of **TAB** both in solution and PMMA film. The unique absorption (band I) and fluorescence spectra of **TAB**, which are completely different from those of anthracene itself, were assigned to the transition between the ground and CT excited states. It was also demonstrated that the lowest-energy absorption accompanied the dipole moment change with 7.8−8.0 D, which proved that the excited state of **TAB** was localized primarily on the p orbital of the boron atom. In practice, our theoretical calculations indicated that the amount of charge transferred from the anthryl group to the p orbital of the boron atom was ∼1.0. Such results explain very well the large solvent dependences of the fluorescence and excited-state properties of **TAB**: fluorescence maximum energy, quantum yield, and lifetime.[1] Furthermore, curious behaviors of the electroabsorption and electrofluorescence spectra, showing dipole moment and molecular polarizability changes, respectively, were explained reasonably by assuming the excited electronic states of **TAB** predicted by the present theoretical considerations. As documented in various papers, boron-containing π-conjugated systems show very interesting optical and redox properties.[19−23] Nonetheless, the works so far reported are directed toward synthetic and materials chemistry. Clearly, both the chemical/physical experiments and the theoretical studies of such systems are very promising for further advances in related studies and systems.

Acknowledgment. The authors acknowledge a Grant-in-aid for Scientific Research from the Ministry of Education, Culture, Sports, Science and Technology (MEXT) of the Japanese Government for the support of the research (Nos. 138530004 and 14050001 to N.K. and No. 15205001 to N.O.).

References and Notes

(1) Part I of this series: Kitamura, N.; Sakuda, E. *J. Phys. Chem. A* **2005**, *109*, 7429.
(2) Suppan, P.; Ghoneim, N. *Solvatochromism*; The Royal Society of Chemistry: Cambridge, U.K., 1997.
(3) Ohta, N.; Okazaki, S.; Yamazaki, I. *Chem. Phys. Lett.* **1995**, *229*, 394.
(4) Umeuchi, S.; Nishimura, Y.; Yamazaki, I.; Murakami, H.; Yamashita, M.; Ohta, N. *Thin Solid Films* **1997**, *311*, 239.
(5) Ohta, N. *Bull. Chem. Soc. Jpn.* **2002**, *75*, 1637.
(6) Ponder, M.; Mathies, R. *J. Phys. Chem.* **1983**, *87*, 5090.
(7) Liptay, W. *Excited States*; Lim, E. C., Ed.; Academic Press: New York, 1974, p 129.
(8) Oh, D. H.; Sano, M.; Boxer, S. G. *J. Am. Chem. Soc.* **1991**, *113*, 6880.
(9) Walters, K. A.; Kim, Y.-J.; Hupp, J. T. *Inorg. Chem.* **2002**, *41*, 2909.
(10) Jalviste, E.; Ohta, N. *J. Chem. Phys.* **2004**, *121*, 4730.
(11) Barnett, G. P.; Kurzmack, M. A.; Malley, M. M. *Chem. Phys. Lett.* **1973**, *23*, 237.
(12) Ramsey, B. G. *J. Phys. Chem.* **1966**, *70*, 611.
(13) Ramsey, B. G.; El-Bayoumi, M.; Kasha, M. *J. Phys. Chem.* **1961**, *35*, 1502.
(14) Ramsey, B. G.; Leffler, J. E. *J. Phys. Chem.* **1963**, *67*, 2242.
(15) Miller, D. S.; Leffler, J. E. *J. Phys. Chem.* **1970**, *74*, 2571.
(16) Yamaguchi, S.; Akiyama, S.; Tamao, K. *J. Am. Chem. Soc.* **2000**, *122*, 6335.
(17) Yamaguchi, S.; Akiyama, S.; Tamao, K. *J. Organomet. Chem.* **2002**, *652*, 3.
(18) Turro, N. J. *Modern Molecular Photochemistry*; Benjamin/Cummings: Menlo Park, CA, 1978.
(19) Yamaguchu, S.; Shirasaka, T.; Tamao, K. *Org. Lett.* **2000**, *2*, 4129.
(20) Yamaguchi, S.; Akiyama, S.; Tamao, K. *J. Am. Chem. Soc.* **2001**, *123*, 11372.
(21) Yamaguchi, S.; Shirasaka, T.; Akiyama, S.; Tamao, K. *J. Am. Chem. Soc.* **2002**, *124*, 8816.
(22) Yamaguchi, S.; Akiyama, S.; Tamao, K. *Organometallics* **1998**, *17*, 4347.
(23) Yamaguchi, S.; Akiyama, S.; Tamao, K. *J. Am. Chem. Soc.* **2000**, *122*, 6793.